Analyst

PAPER

View Article Online
View Journal

Cite this: DOI: 10.1039/c9an00843h

Robust and highly specific fluorescence sensing of *Salmonella typhimurium* based on dual-functional phi29 DNA polymerase-mediated isothermal circular strand displacement polymerization

Shasha Li,[a] Su Liu,[b] Yicheng Xu,[a] Rufeng Zhang,[b] Yihan Zhao,[a] Xiaonan Qu,[b] Yu Wang,*[a] Jiadong Huang[a,c] and Jinghua Yu[c]

A simple and robust fluorescence sensing strategy has been developed for the detection of pathogenic bacteria by the combination of the dual functionality of phi29 DNA polymerase with isothermal circular strand displacement polymerization (ICSDP). The strategy relies on target-triggered formation of a mature primer that initiates the cyclic strand displacement polymerization reaction with the aid of dual functional phi29; thus, amplified detection of the target can be achieved. To our knowledge, this work is the first report where dual functional phi29-assisted ICSDP has been employed for fluorescence sensing of pathogenic bacteria. It is worth noting that a hairpin pre-primer is introduced that can be trimmed into a mature primer for initiating ICSDP *via* the 3′ → 5′ proofreading exonuclease activity of phi29, which contributes to the ultrahigh specificity of the strategy owing to the elimination of the unwished nonspecific extension. On the basis of the present amplification strategy, our biosensor exhibits excellent specificity and sensitivity toward *S. typhimurium* with an excellent detection limit as low as 1.5 cfu mL^{-1}. In addition, the strategy offers the advantages of a simplified operation, shortened analysis time, and highly sensitive detection of pathogens with only a one-step reaction. Furthermore, by redesigning the corresponding binding molecules, the proposed strategy can be easily extended for the detection of a wide spectrum of analytes. Hence, the dual functional phi29-assisted ICSDP strategy indeed creates a robust and convenient fluorescence sensing platform for the identification of pathogenic bacteria and related food safety analysis.

Received 9th May 2019,
Accepted 14th June 2019

DOI: 10.1039/c9an00843h

rsc.li/analyst

1. Introduction

In recent years, diseases caused by food-borne pathogenic bacteria have become a serious threat to public health and food safety.[1] According to the World Health Organization (WHO), food-borne pathogens result in approximately 600 million illnesses and 420 000 deaths per year.[2] Therefore, there is an urgent need for the development of rapid and sensitive assay methods for the detection of pathogenic bacteria. The conventional method for the identification of pathogens is dependent on culture and colony counting that takes at least a few days to get the results.[3,4] Nowadays, some appealing techniques including polymerase chain reaction (PCR),[5] enzyme-linked immunosorbent assay (ELISA),[6] surface plasmon resonance (SPR),[7] electrochemical impedance spectroscopy (EIS),[8] and other detection techniques,[9–11] have been extensively explored for the determination of pathogens. Although these methods enable the detection of pathogens with a high sensitivity and specificity, they might suffer from the shortcomings of time-consuming processes, tedious operation, expensive instrumentation, and the need for trained technicians.[12] Accordingly, it is imperative to develop rapid, convenient, and low cost assay methods for the detection of pathogenic bacteria with a high sensitivity and accuracy to guarantee public health and food safety.

Recently, a wider variety of isothermal nucleic acid amplification techniques have been generally employed in order to improve the sensitivity of the target molecule assay under mild conditions, such as rolling circle amplification (RCA),[13–15] exonuclease or endonuclease-assisted signal amplification,[16,17] isothermal circular strand displacement polymerization (ICSDP),[18,19] loop-mediated isothermal amplification (LAMP),[20] and hybridization chain reaction (HCR).[21] On account of the advantages of adaptability, undemanding

[a]College of Biological Sciences and Technology, University of Jinan, Jinan 250022, P. R. China. E-mail: bio_wangy@ujn.edu.cn; Fax: +86-531-82769122; Tel: +86-531-89736122
[b]School of Water Conservancy and Environment, University of Jinan, Jinan 250022, P. R. China
[c]Key Laboratory of Chemical Sensing & Analysis in Universities of Shandong, College of Chemistry and Chemical Engineering, University of Jinan, Jinan 250022, P. R. China

design, and high amplification efficiency, ICSDP has attracted increasing attention in biosensing and bioimaging analysis.[22] ICSDP relies on nicking the endonuclease-aided isothermal polymerization reaction activated by the annealing of a specific primer with a single-stranded template in the presence of polymerase. During the polymerization, the bound target can be displaced and the secondary target can be continuously generated, which promotes more rounds of the polymerization reaction that in turn achieves amplified detection of the target. So far, ICSDP has been widely used for diverse detection of analytes including nucleic acids, proteins, small molecules, and heavy metal ions. For example, Yang and co-authors reported a facile sensing strategy for the quantification and intracellular imaging of microRNAs in living cells based on branched DNA junction-enhanced ICSDP.[23] Huang and co-authors developed a new fluorescence polarization aptasensor for highly sensitive detection of proteins using cascade strand displacement amplification and polystyrene nanoparticle enhancement.[24] Song and co-authors demonstrated a new amplified fluorescence aptameric sensor for detecting adenosine triphosphate based on isothermal circular strand-displacement polymerization amplification.[25] Li and co-authors reported a DNAzyme and isothermal strand displacement signal amplification-based method for the quantification of lead(II) ions.[26] However, to date, the technique has not been studied in any attempts for its use in a pathogenic bacteria assay.

Herein, we develop a robust and highly specific fluorescence sensing strategy for the detection of pathogenic bacteria using dual-functional phi29 DNA polymerase-mediated ICSDP. In our assay, a fluorescence-quenched hairpin probe (HAP2) is skillfully designed that functions not only as a pre-primer for initiating ICSDP but also as an indicator for the fluorescence signal output. This design of the hairpin pre-primer can effectively avoid the unwished extension attributed from the dynamic contact between the single-stranded primer with the template; thus, the ultrahigh specificity of our strategy can be achieved for the identification of pathogenic bacteria. Additionally, except for the processive synthesis property, the $3' \rightarrow 5'$ proofreading exonuclease activity of phi29 is especially utilized to induce the formation of a mature primer for ICSDP. On the basis of the combination of ICSDP with the dual functionality of phi29,[27,28] our strategy offers the advantages of a simplified operation, shortened analysis time, and highly sensitive detection of pathogens with only a one-step reaction. Therefore, our proposed strategy might create a robust and convenient sensing platform for the detection of pathogenic bacteria and related food safety analysis.

2. Experimental section

2.1 Materials and reagents

All sequences whose oligonucleotides are listed in Table 1 were HPLC-purified and synthesized by Sangon Biotechnology Co. Ltd (Shanghai, China). Phi29 DNA polymerase (phi29) and nicking endonuclease *Nt. AlwI* (*Nt. AlwI*) were purchased from New England Biolabs (Ipswich, MA, USA). Deoxyribonucleoside triphosphates (dNTPs) were purchased from Takara Biotechnology Co., Ltd (Dalian, China). *Salmonella typhimurium* (KCTC 1925), *Escherichia coli* (KCTC 2571), *Bacillus subtilis* (KCTC 1028) and *Listeria* (KCTC 3569) were obtained from the Institute of Microbiology Chinese Academy (Beijing, China). Peptone, beef extract powder, bacto-tryptone and bacto-yeast extract were obtained from Qingdao Biological Technology Co. Ltd (Qingdao, China). Agarose, DNA ladder marker and TAE buffer were purchased from Sangon Biotech Co., Ltd (Shanghai, China). Other chemicals were of analytical grade and were used without further purification. Ultrapure water obtained from a Millipore Milli-Q water purification system was used throughout.

Table 1 DNA oligonucleotide sequence used in this work

Oligonucleotide name	Sequence (5′–3′) description
Apt	AGTAATGCCCGGTAGTTATTCAAAGATGAGTAGGAAAAGA
T	TCTTTTCCTAGAAATCCGGGCATTACT
HAP1	**AGTAATGCCCGG***CTTAGATCCC*CTGTCCATTACT
HAP2	Dabcyl-GGAGAAGTTTATTTCTTAGTTTCTAGTAATGGACGTTCTTCTCC-FAM

The underlined bases in the aptamer (Apt) are matched bases with T. The three functional regions of the designed HAP1 are marked in three different forms. The recognition region is highlighted in bold black, the nicking region is highlighted in italics, the primer region is highlighted by an underline. HAP2 is labeled with 4-(4-dimethylaminophenyl) diazenylbenzoic acid (Dabcyl) quencher and fluorescein isothiocyanate (FAM) fluorophore and the bases highlighted by an underline could hybridize with the bases underlined in HAP1.

2.2 Apparatus

Gel electrophoresis was conducted using a DYCZ-24DN electrophoresis cell (LIUYI, Beijing, China) and a Bio-Rad Gel imaging system (Bio-Rad, USA). Fluorescence spectra were recorded using an Agilent Cary Eclipse spectrofluorometer (Agilent, USA) with excitation at 494 nm. The slit was set to be 5 nm for both the excitation and emission.

2.3 Cultivation of bacterial strains

The bacterial culture was routinely grown at 37 °C in a Luria–Bertani medium for 12 h. The bacterial cells in logarithmic growth were obtained and centrifuged at 800 rpm for 5 min and then rinsed twice with phosphate buffer saline (PBS, 10 mM, pH 7.4). The sediment was resuspended in PBS solution to obtain a homogeneous cell suspension. The bacterial number was determined by the plate counting method.

2.4 *S. Typhimurium* detection

All samples were prepared in Tris-HCl reaction buffer (50 mM, pH 7.9 containing 20 mM Tris-acetate and 10 mM magnesium acetate) for the detection of *S. typhimurium* and the detailed procedure was as follows: firstly, the same volumes of Apt (100 μM) and T (100 μM) were sufficiently mixed and incubated at 95 °C for 5 min. Then, the mixture was cooled down to

room temperature and stored at −20 °C until use. Subsequently, Apt–T hybrid duplex (3 μL, 10 μM), HAP1 (1.5 μL, 100 μM), HAP2 (1.5 μL, 100 μM), phi29 DNA polymerase (3 μL, 10 U μL^{-1}), dNTPs (3 μL, 10 mM), *Nt.AlwI* (3 μL, 10 U μL^{-1}), CutSmart (3 μL, 10×) and 3 μL of *S. typhimurium* (or other food-borne diseases) with different concentrations were mixed and incubated at 37 °C for 90 min. Finally, the above reaction solution (30 μL) was mixed with 70 μL of ultrapure water and scanned using an Agilent Cary Eclipse spectrofluorometer. Unless otherwise noted, all experiments for *S. Typhimurium* measurements were repeated three times.

2.5 Polyacrylamide gel electrophoresis (PAGE) analysis

The products of this amplification strategy were characterized using 15% PAGE. In the PAGE assay, electrophoresis was carried out at 100 V in 1× TBE (50 mM Tris Borate, 2.0 mM EDTA, pH 8.2) buffer for 80 min at room temperature and stained for 30 min in a 1× GelRed solution. After electrophoresis, the gel was visualized *via* fluorescence detection using a Bio-Rad Gel imaging system.

3. Results and discussion

3.1 Principle of the proposed ICSDP strategy for the pathogenic bacteria assay

The working principle of the proposed fluorescence sensing strategy for the ultrasensitive detection of pathogenic bacteria is illustrated in Scheme 1. *Salmonella typhimurium* (*S. typhimurium*) was chosen as a model analyte. The reaction system is comprised of five elements: an arched probe used for the recognition of target *S. typhimurium*, a hairpin probe 1 (HAP1) that affords the template of ICSDP, a fluorescence-quenched hairpin probe 2 (HAP2) functioned as the pre-primer for ICSDP and the indicator for the fluorescence signal output, and two nucleic acid enzymes that are phi29 DNA polymerase and nicking endonuclease *Nt. AlwI*, respectively. The arched probe consists of the anti-*S. typhimurium* aptamer and a trigger (T) that can anneal with the 5′ end of HAP1. HAP1 is skillfully designed to contain a trigger-annealing sequence (T*), a specific recognition sequence for *Nt. AlwI* (R*), and a DNA segment complementary to the loop of HAP2 (S*). In the assay of *S. typhimurium*, the specific recognition of *S. typhimurium* and the aptamer leads to the release of T, which can bind to the 5′ terminus of HAP1 that induces the conformation switch of HAP1. Immediately, the exposed 3′ terminus of HAP1 attaches with the loop of HAP2 (S) and functions as a primer to initiate an extension reaction by utilizing HAP2 as the template in the presence of phi29 and dNTPs. In the meantime, since the newly liberated tail of HAP2 (L) is unmatched with that of HAP1, the unpaired base can be digested *via* the processive 3′ → 5′ exonuclease activity of phi29;[29–31] thus, the trimmed 3′ end of HAP2 can act as a mature primer for initiating the strand displacement polymerization reaction. In the process of polymerization, T is dis-

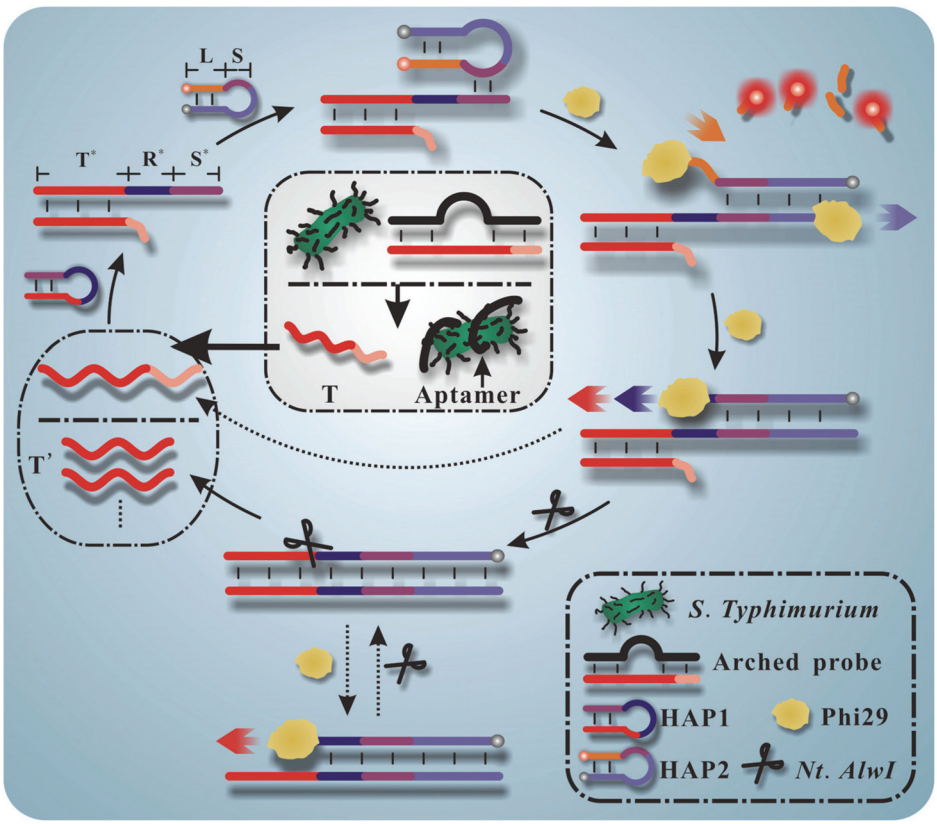

Scheme 1 Schematic illustration of the fluorescence sensing of *S. typhimurium* using dual-functional phi29 DNA polymerase-mediated ICSDP.

placed and a recognition site for *Nt. AlwI* is generated in the DNA duplex; thus, *Nt. AlwI* nicked the site and induced the formation of single-stranded DNA fragments (secondary T, T′). Subsequently, the detached T and T′ can combine with HAP1, promoting more rounds of strand displacement polymerization reaction; thus, numerous T′ are continuously produced. Eventually, more and more HAP2 is opened, in which a remarkably enhanced fluorescence signal can be obtained due to the detachment of the fluorophore (FAM) from the quencher (Dabcyl). Hence, our ICSDP-based strategy holds great potential for providing a robust and convenient tool for detecting *S. typhimurium* with ultrahigh specificity.

3.2 Feasibility of the strategy for the *S. Typhimurium* assay

In order to verify the feasibility of our proposed strategy, a series of control experiments were investigated, and the results are depicted in Fig. 1. When the system was incubated with *S. typhimurium*, a significantly strong fluorescence signal was observed with an emission peak at 519 nm (curve a). In contrast, it was found that a negligible fluorescence response was obtained for the blank sample, signifying a desirable signal-to-background ratio of 20.1 (curve b). These data indicated the specific recognition of *S. typhimurium* and aptamer initiated dual functional phi29-mediated ICSDP, resulting in the trimming of HAP2 that in return released a remarkably enhanced fluorescence signal. When the system was incubated with *S. typhimurium* in the absence of phi29, we observed a very weak fluorescence response similar to that of the blank sample, manifesting that the circular strand displacement reaction was activated by the phi29-assisted extension reaction (curve c). When the system was incubated with *S. typhimurium* in the absence of *Nt. AlwI*, a moderate fluorescence signal was obtained, suggesting that a certain amount of HAP2 was opened due to the phi29-assisted trigger (T) recycle amplification (curve d). In addition, after incubation with the arched probe, HAP2, phi29, and *Nt. AlwI* with *S. typhimurium*, there was a dinky fluorescence peak, which demonstrated that the conformation switch of HAP2 was induced by the attachment of the exposed 3′-end of HAP1 with the loop of HAP2, rather than instability or other factors (curve e). Furthermore, when the target *S. typhimurium* was replaced by non-target pathogenic bacteria *E. coli*, it was observed that an extremely weak fluorescence signal was obtained, confirming that the remarkably enhanced fluorescence signal was triggered by the specific interaction of the target and aptamer (curve f). On the basis of the above results, it was reasonably concluded that the proposed strategy could be applied for the quantitative assay of *S. typhimurium* with a high specificity.

3.3 PAGE analysis

PAGE analysis was carried out to directly certify the reaction mechanism of the ICSDP process, and the results are depicted in Fig. 2. It was observed that the arched probe gave a bright band at Lane 1, while the trigger (T) gave a relatively weak band at Lane 2 due to the poor dye-ability of single-stranded DNA. Lanes 3 and 4 displayed bright bands of our designed HAP1 and HAP2, respectively. When the arched probe, HAP1, and HAP2 were incubated with *S. typhimurium*, the brightness of the band at the position of HAP1 was visibly decreased, and a band with an obviously increased brightness appeared on the image (lane 5). This indicated the specific recognition of *S. typhimurium* and the aptamer resulted in the detachment of T from the arched probe that could anneal with HAP1. Because the molecular weight of the produced T-HAP1 duplex was similar to that of HAP2, it was difficult to separate the two bands. When the arched probe, HAP1, HAP2, and phi29 were incubated with *S. typhimurium*, we observed three

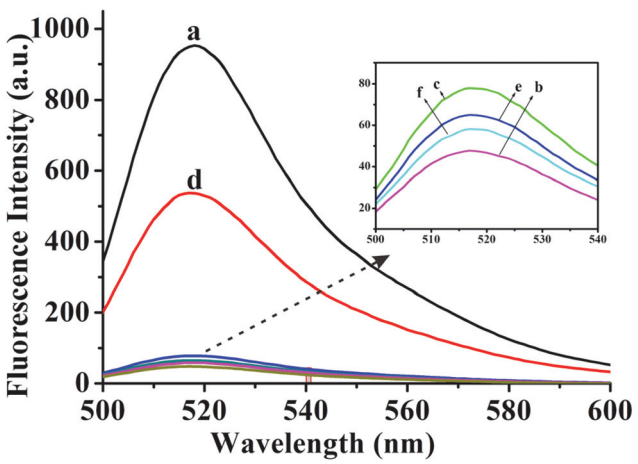

Fig. 1 Fluorescence emission spectra responses of the biosensor in the presence of 5.0×10^5 cfu mL^{-1} *S. typhimurium* (a). Curves b to f are for the control experiments which are performed without *S. typhimurium* (b), without phi29 (c), without *Nt. AlwI* (d), without HAP1 (e), and non-target pathogenic bacteria *E. coli* in place of *S. Typhimurium* (f).

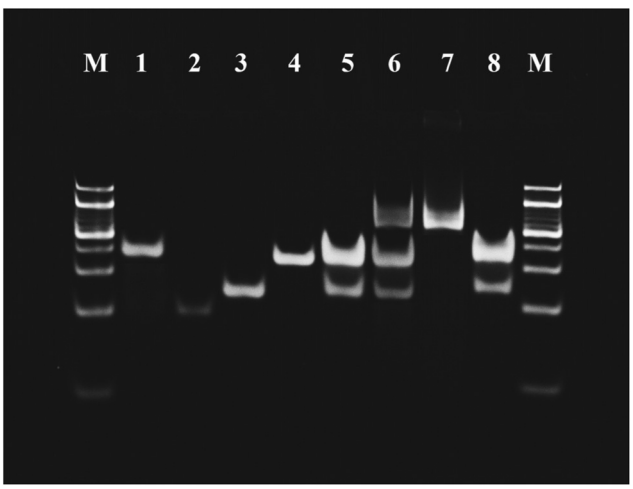

Fig. 2 Gel electrophoresis image of the ICSDP reaction. Lane M, DNA marker; Lane 1, arched probe; Lane 2, arched probe incubated with *S. typhimurium*; Lane 3, HAP1; Lane 4, HAP2; Lane 5, arched probe incubated with HAP1, HAP2, and *S. typhimurium*; Lane 6, arched probe incubated with HAP1, HAP2, phi29, and *S. typhimurium*; Lane 7, the positive sample; and Lane 8, the blank sample.

bands on the image. The brightness of the bottom two bands was remarkably decreased compared to the corresponding bands of lane 5, and a new band with a slower migration rate appeared (lane 6). This demonstrated that HAP1 could be immediately extended with the aid of phi29 when HAP1 combined to HAP2; thus, HAP1 and HAP2 were continually consumed due to the cyclic utilization of T, inducing the formation of duplex DNA. When the arched probe, HAP1, HAP2, phi29, and *Nt. AlwI* were incubated with *S. typhimurium*, there was a bright band with the same mobility with that of the top band at lane 6, implying that HAP1 and HAP2 were depleted and a large amount of DNA duplex was produced after the circular strand displacement reaction process (lane 7). In contrast, for the blank sample, it was found that lane 8 displayed distinct bands characteristic for the arched probe, HAP1, and HAP2. These data gave immediate evidence that the binding of the target and aptamer activated the ICSDP process and the accompanied consumption of HAP.

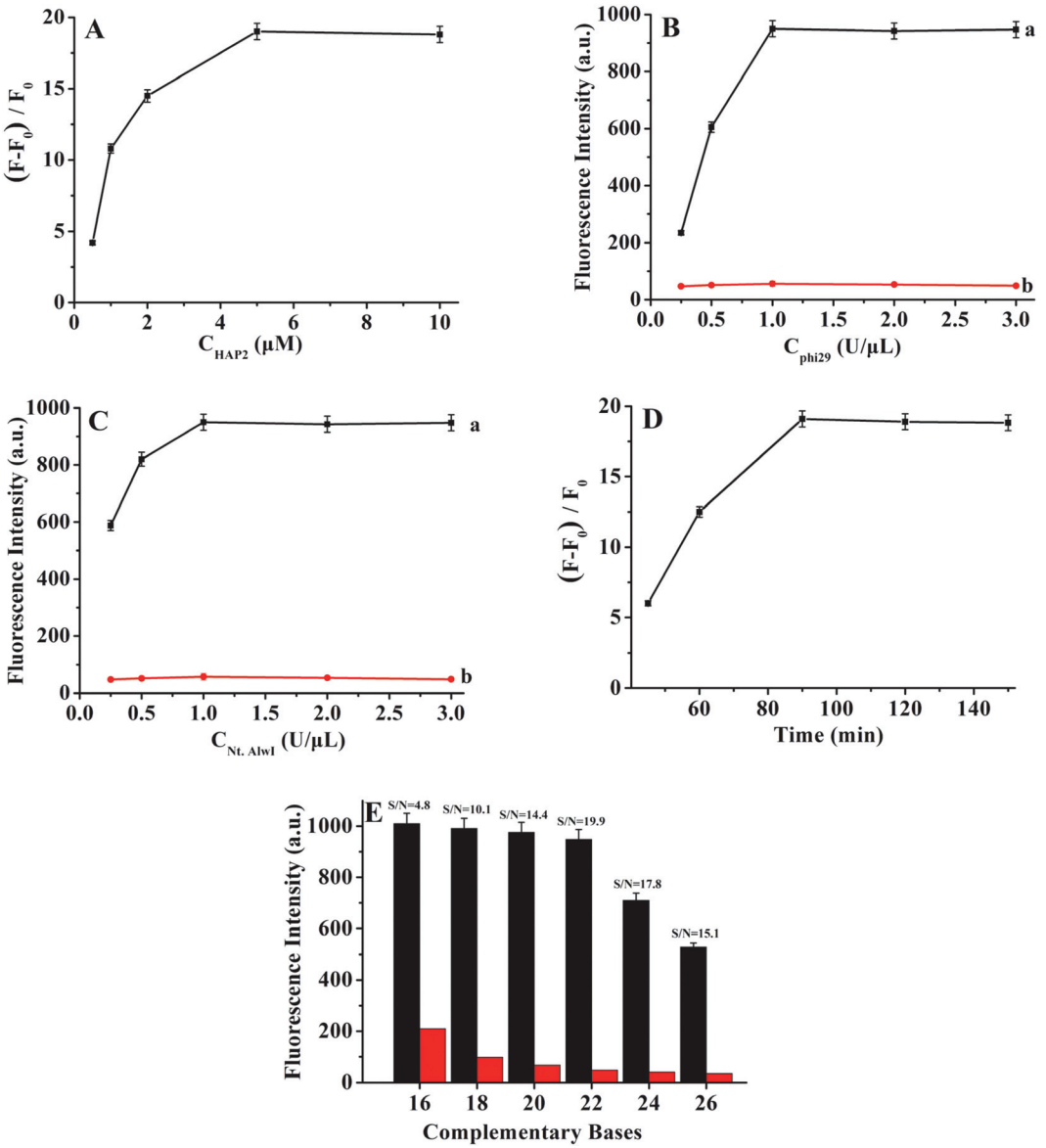

Fig. 3 (A) Effect of the concentration of HAP2 on the $(F - F_0)/F_0$ value of the biosensor, F and F_0 represent the fluorescence intensity at 519 nm of the biosensor in the presence and absence of 5.0×10^5 cfu mL^{-1} *S. typhimurium*, respectively; (B) effects of the concentration of phi29 on the fluorescence intensity at 519 nm of the biosensor in the presence (curve a) and absence (curve b) of 5.0×10^5 cfu mL^{-1} *S. typhimurium*; (C) effects of the concentration of *Nt. AlwI* on the fluorescence intensity at 519 nm of the biosensor in the presence (curve a) and absence (curve b) of 5.0×10^5 cfu mL^{-1} *S. typhimuriumis*; (D) effects of the reaction time on the $(F - F_0)/F_0$ value of the biosensor, F and F_0 represent the fluorescence intensity at 519 nm of the biosensor in the presence and absence of 5.0×10^5 cfu mL^{-1} *S. typhimurium*, respectively; and (E) effect of the complementary bases of Apt and T on the fluorescence intensity at 519 nm of the biosensor in the presence (the black bar) and absence (the red bar) of 5.0×10^5 cfu mL^{-1} *S. typhimurium*. The error bars are standard deviations across three repetitive experiments.

3.4 Optimization of experimental conditions

In order to acquire optimal analytical performance of the biosensor, some key experimental parameters including the concentration of HAP2, the amounts of phi29 and *Nt. AlwI*, the reaction time for ICSDP, and the complementary bases of Apt and T were orderly investigated (Fig. 3). Since HAP2 functions not only as the pre-primer for the ICSDP reaction but also as the tracer for the fluorescence signal output, the concentration of HAP2 was optimized, and the results are shown in Fig. 3A. We observed that the $(F - F_0)/F_0$ value gradually increased with the increasing of the HAP2 concentration and experienced almost no chance when the concentration was 5 μM. Thus, 5 μM was selected as the optimal concentration in the following experiments. Additionally, the amounts of phi29 and *Nt. AlwI* had a great impact on the amplification efficiency of the ICSDP reaction. The concentrations of phi29 and *Nt. AlwI* were also optimized on the basis of the fluorescence signal intensity in the presence and absence of 5.0×10^5 cfu mL^{-1} *S. typhimuriumiss*, and the results are depicted in Fig. 3B and C, respectively. As shown in Fig. 3B, for the positive sample, the fluorescence intensity was continuously intensified with the increasing of the concentration of phi29 and reached equilibrium when the concentration reached 1 U μL^{-1}, while the fluorescence intensity was nearly unchanged for the blank sample. Therefore, 1 U μL^{-1} was chosen as the optimal concentration. Similarly, it was observed from Fig. 3C that the optimized concentration of *Nt. AlwI* was 1 U μL^{-1} for the ICSDP reaction. Furthermore, the ICSDP reaction time was studied by probing the $(F - F_0)/F_0$ value in the presence and absence of 5.0×10^5 cfu mL^{-1} *S. typhimuriumiss* (Fig. 3D). We observed that the $(F - F_0)/F_0$ value increased with the increase of the reaction time and reached a plateau at 90 min. Hence, 90 min was adopted as the optimum reaction time for the subsequent experiments. In addition, the complementary sequence of Apt and T is also crucial in our assay. To obtain the highest signal-to-noise (S/N), the complementary bases of Apt and T were optimized, and the results are shown in Fig. 3E. It was found that the fluorescence signal intensity was gradually decreased with the increase of the complementary bases for the positive sample. However, for the blank sample, the fluorescence intensity was continuously decreased upon an increase of the complementary bases and reached equilibrium when the bases were 22. The highest S/N was obtained when the bases were 22. Thus, 22 bases were chosen as the optimal complementary bases in the following experiments.

3.5 Analytical performance for *S. Typhimurium* detection

Under the optimized experimental conditions, the analytical performance of the constructed biosensor was investigated towards *S. typhimurium* detection at various concentrations by fluorescence spectroscopy. As seen from Fig. 4A, the fluorescence intensities at 519 nm increased significantly with the increasing of the concentrations of *S. typhimurium* from 0 to 5.0×10^5 cfu mL^{-1}. Fig. 4B displayed a good linear correlation to the logarithm (log) of the *S. typhimurium* concentration ranging from 10 cfu mL^{-1} to 5.0×10^5 cfu mL^{-1}. The linear regression equation was $F = -142.742 + 190.040 \times \lg C_{S.\ Typhimurium}$ with a correlation coefficient of 0.996. The detection limit was calculated to be 1.5 cfu mL^{-1} in terms of the rule of 3 times standard deviation over the blank response. Additionally, the analytical performance of our biosensor for the quantitative assay of *S. typhimurium* was in comparison with that of the previous reported methods, and the results are shown in Table 2. It was found that the sensitivity of the biosensor was superior to the majority of the existing methods for *S. typhimurium* quantification. Besides, our ICSDP-based fluorescence sensing strategy allowed robust, convenient, and one-step homogenous detection of *S. typhimurium* with ultrahigh specificity.

3.6 Detection specificity

To evaluate the specificity of the present strategy for the *S. typhimurium* assay, the biosensor was challenged with target *S. typhimurium* and other non-target pathogenic bacteria including *Listeria*, *E. coli*, and *Bacillus subtilis*. The results are shown in Fig. 5. As expected, the biosensor only showed a sig-

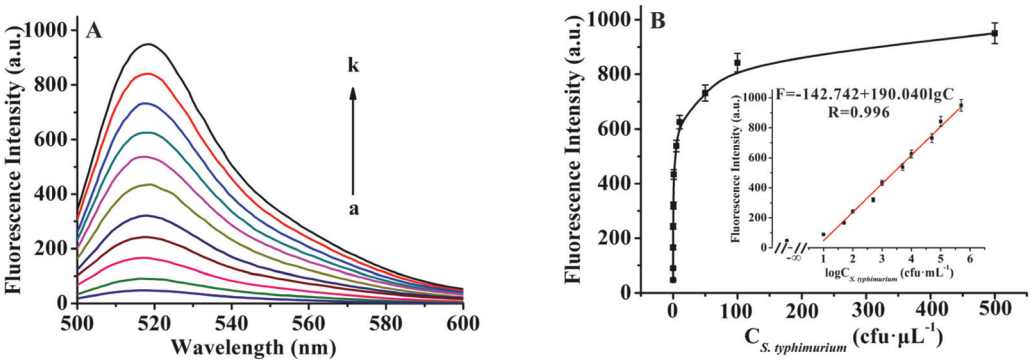

Fig. 4 (A) Fluorescence spectra responses to different concentrations of *S. typhimurium* (from curve a to k: 0, 10, 50, 1.0×10^2, 5.0×10^2, 1.0×10^3, 5.0×10^3, 1.0×10^4, 5.0×10^4, 1.0×10^5, and 5.0×10^5 cfu mL^{-1}) and (B) the calibration curve of fluorescence intensity at 519 nm for different *S. typhimurium* concentrations. The inset is the plot of the fluorescence intensity at 519 nm *versus* the logarithm value of the *S. typhimurium* concentration. The error bars show the standard deviations of three repetitive experiments.

Table 2 Comparison of different assay methods for the detection of pathogenic bacteria

Methods	Detection range (cfu mL^{-1})	Detection limit (cfu mL^{-1})	Detection time	Ref.
Immunoassays	8×10^1–8×10^8	8.0×10^1	4.5 h	32
Colorimetric assay	8×10^3–8×10^7	1.0×10^3	1.5 h	33
Chemiluminescence	5×10^2–5×10^5	1.0×10^2	3.0 h	34
Electrochemical assay	6×10^2–6×10^6	6.0×10^2	4.5 h	35
Sandwich fluorescence	1×10^3–1×10^9	2.0×10^2	3.0 h	36
Polymerase chain reaction	1×10^1–1×10^2	1.0×10^1	2.0 h	37
Surface plasmon resonance	2×10^1–1×10^2	2.0×10^1	10 h	38
Fluorescence assay	1×10^4–1×10^8	5.0×10^1	1.5 h	39
Sandwich immunoassays	1×10^4–1×10^6	5.4×10^3	2.0 h	40
Fluorescence assay	1×10^1–5×10^5	1.5×10^0	1.5 h	This work

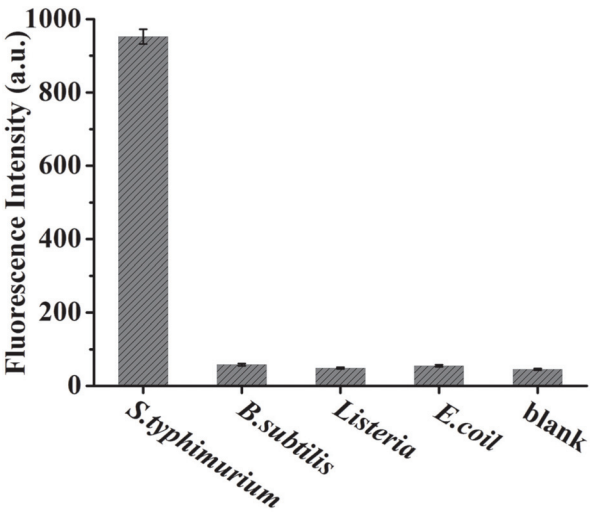

Fig. 5 The fluorescence responses at 519 nm obtained for our biosensor towards the detection of different pathogenic bacteria. The concentration of *S. Typhimurium* is 5.0×10^5 cfu mL^{-1}. The concentration of non-target bacteria is 5.0×10^6 cfu mL^{-1}. The error bars are standard deviations across three repetitive experiments.

nificantly strong fluorescence response in the presence of target *S. typhimurium*, while the fluorescence response to several non-target bacteria was on the edge of that of the blank sample. These results distinctly confirmed the excellent specificity of the constructed biosensor for the *S. typhimurium* assay.

3.7 Real sample analysis

To evaluate the applicability of this biosensor in complicated matrixes, the quantitative assay of *S. typhimurium* in spiked milk samples was considered. Different concentrations of *S. typhimurium* were successively added into the milk samples that were detected without pretreatment except for dilution with the reaction buffer. To assess the accuracy of our assay, a classic plate count method was also used for analyzing the spiked samples. As shown in Table 3, these data obtained by our method had no obvious discrepancies compared to those obtained *via* the plate count method, and the discrepancies between the two methods were all smaller than 11.5%. In addition, the recovery of the proposed strategy was in the range of 95.1% to 110.1%. These data clearly demonstrated that the proposed strategy could be applied for real sample analysis with a desirable reliability and accuracy.

4. Conclusions

In summary, we report the development of a simple, rapid, and convenient fluorescence sensing strategy for highly sensitive and specific detection of pathogenic bacteria. The strategy relies on target-triggered formation of a mature primer that initiates the cyclic strand displacement polymerization reaction; thus, amplified detection of the target can be achieved due to the combination of the dual functionality of phi29 with the high efficiency of ICSDP. This work is to our knowledge the first time that dual functional phi29-assisted ICSDP has been integrated into fluorescence sensing of pathogenic bacteria. On the basis of the amplification strategy, the biosensor allows to detect *S. typhimurium* with an excellent detection limit as low as 1.5 cfu mL^{-1}, which is better than most of the existing methods. Additionally, our biosensor offers the advantages of ultrahigh specificity, simplified operation, and shor-

Table 3 *S. typhimurium* analysis in real samples

	Measured (cfu mL^{-1})		Recovery (%) ± SD	
Spiked amount (cfu mL^{-1})	Our method	Plate count method	Our method	Plate count method
1×10	$(1.087 \pm 0.014) \times 10$	$(0.976 \pm 0.027) \times 10$	108.7 ± 1.4	97.6 ± 2.7
1×10^2	$(0.986 \pm 0.027) \times 10^2$	$(0.968 \pm 0.037) \times 10^2$	98.6 ± 2.7	96.8 ± 3.7
1×10^3	$(1.023 \pm 0.009) \times 10^3$	$(1.017 \pm 0.025) \times 10^3$	102.3 ± 0.9	101.7 ± 2.5
1×10^4	$(1.028 \pm 0.018) \times 10^4$	$1.037 \pm 0.017) \times 10^4$	102.8 ± 1.8	103.7 ± 1.7
1×10^5	$(0.982 \pm 0.031) \times 10^5$	$(0.994 \pm 0.028) \times 10^5$	98.2 ± 3.1	99.4 ± 2.8

tened analysis time. Furthermore, the proposed strategy can be easily extended for the detection of other analytes by re-designing the corresponding binding molecules. Therefore, the dual functional phi29-assisted ICSDP strategy indeed creates a useful and practical platform for the detection of pathogenic bacteria and related food safety analysis.

Conflicts of interest

There are no conflicts to declare.

Acknowledgements

This work was supported by the National Natural Science Foundation of China (31471644), the Primary Research & Development Plan of Shandong Province (2017GSF220009), and the Program for Taishan Scholars of Shandong Provinces (ts201712048).

References

1 J. Wu, R. Wang, Y. Lu, M. Jia, J. Yan and X. Bian, *Anal. Chem.*, 2019, **91**, 1027–1033.
2 H. Yousefi, M. M. Ali, H. M. Su and C. D. M. Filipe, *ACS Nano*, 2018, **12**, 3287–3294.
3 L. Li, Q. Li, Z. Liao, Y. Sun, Q. Cheng and Y. Song, *Anal. Chem.*, 2018, **90**, 9621–9628.
4 T. Kinoshita, K. Ishiki, D. Q. Nguyen and H. Shiigi, *Anal. Chem.*, 2018, **90**, 4098–4103.
5 Y. Tsuchido, R. Horiuchi and T. Hashimoto, *Anal. Chem.*, 2019, **91**, 3929–3935.
6 H. Peng and I. A. Chen, *ACS Nano*, 2019, **13**, 1244–1252.
7 J. Chen, Z. Huang, Z. Luo, Q. Yu, Y. Xu, X. Wang, Y. Li and Y. Duan, *Anal. Chem.*, 2018, **90**, 12019–12026.
8 W. Lee, D. Kwon, B. Chung, G. Y. Jung, A. Au, A. Folch and S. Jeon, *Anal. Chem.*, 2014, **86**, 6683–6688.
9 H. Shen, J. Wang, H. Liu, Z. Li, F. Jiang, F. B. Wang and Q. Yuan, *ACS Appl. Mater. Interfaces*, 2016, **8**, 19371–19378.
10 P. Rajapaksha, A. Elbourne, S. Gangadoo, R. Brown, D. Cozzolino and J. Chapman, *Analyst*, 2019, **144**, 396–411.
11 H. J. Kim, C. Kwon, B. S. Lee and H. Noh, *Analyst*, 2019, **144**, 2248–2255.
12 O. Lazcka, F. J. Del Campo and F. X. Munoz, *Biosens. Bioelectron.*, 2007, **22**, 1205–1217.
13 Q. Yao, Y. Wang and J. Wang, *ACS Nano*, 2018, **12**, 6777–6783.
14 Y. Cheng, X. Zhang, Z. Li, X. Jiao, Y. Wang and Y. Zhang, *Angew. Chem., Int. Ed.*, 2009, **48**, 3268–3272.
15 J. Wang, Y. Wang, S. Liu, H. Wang, X. Zhang, X. Song and J. Huang, *Analyst*, 2018, **143**, 3951–3958.
16 X. Song, Y. Wang, S. Liu, X. Zhang, H. Wang, J. Wang and J. Huang, *Analyst*, 2018, **143**, 5771–5778.
17 W. Xu, X. Xie, D. Li, Z. Yang, T. Li and X. Liu, *Small*, 2012, **8**, 1846–1850.
18 Y. Yao, S. Li, J. Cao, W. Liu and K. Fan, *Chem. Commun.*, 2018, **54**, 4774–4777.
19 C. Ding, X. Li, Y. Ge and S. Zhang, *Anal. Chem.*, 2010, **82**, 2850–2855.
20 H. J. Chun, S. Kim, Y. D. Han, K. R. Kim, J. H. Kim, H. Yoon and H. C. Yoon, *ACS Sens.*, 2018, **3**, 2261–2268.
21 S. Helmig and K. V. Gothelf, *Angew. Chem., Int. Ed.*, 2017, **56**, 13633–13636.
22 Z. Li, W. Zhu, J. Zhang, J. Jiang, G. Shen and R. Yu, *Analyst*, 2013, **138**, 3616–3620.
23 Z. Yang and S. Zhang, *Anal. Chem.*, 2018, **90**, 13891–13899.
24 S. Q. Huang, J. Hu, G. Zhu and C. Y. Zhang, *Biosens. Bioelectron.*, 2015, **65**, 191–197.
25 W. Song, Q. Zhang, X. Xie and S. Zhang, *Biosens. Bioelectron.*, 2014, **61**, 51–56.
26 W. Li, Y. Yang, J. Chen, Q. Zhang, Y. Wang, F. Wang and C. Yu, *Biosens. Bioelectron.*, 2014, **53**, 245–249.
27 X. Y. Li, Y. C. Du, Y. P. Zhang and D. M. Kong, *Sci. Rep.*, 2017, **7**, 6263.
28 Y. C. Du, Y. J. Zhu, X. Y. Li and D. M. Kong, *Chem. Commun.*, 2018, **54**, 682–685.
29 M. Liu, W. Zhang, Q. Zhang, J. D. Brennan and Y. Li, *Angew. Chem., Int. Ed.*, 2015, **54**, 9637–9641.
30 M. Liu, Q. Zhang, D. Chang, J. Gu, J. D. Brennan and Y. Li, *Angew. Chem., Int. Ed.*, 2017, **56**, 6142–6146.
31 M. Liu, Q. Yin and E. M. McConnell, *Chemistry*, 2018, **24**, 4473–4479.
32 C. Cheng, L. Yang, M. Zhong, W. Deng, Y. Tan, Q. Xie and S. Yao, *Analyst*, 2018, **143**, 4067–4073.
33 H. Su, H. Zhao, F. Qiao, L. Chen, R. Duan and S. Ai, *Analyst*, 2013, **138**, 3026–3031.
34 D. Kwon, J. Joo, J. Lee, K. H. Park and S. Jeon, *Anal. Chem.*, 2013, **85**, 7594–7598.
35 Z. Yang, Y. Wang and D. Zhang, *Biosens. Bioelectron.*, 2017, **98**, 248–253.
36 W. Kong, J. Xiong, H. Yue and Z. Fu, *Anal. Chem.*, 2015, **87**, 9864–9868.
37 S. Wu, N. Duan, Z. Shi, C. Fang and Z. Wang, *Anal. Chem.*, 2014, **86**, 3100–3107.
38 H. Zhang, X. Ma, Y. Liu, N. Duan, S. Wu, Z. Wang and B. Xu, *Biosens. Bioelectron.*, 2015, **74**, 872–877.
39 Y. Sun, C. Zhao, Z. Yan, J. Ren and X. Qu, *Chem. Commun.*, 2016, **52**, 7505–7508.
40 P. L. Guo, M. Tang, S. L. Hong, X. Yu, D. W. Pang and Z. L. Zhang, *Biosens. Bioelectron.*, 2015, **74**, 628–636.

